PROTEINS: Structure, Function, and Bioinformatics 68:389–402 (2007)

Superantigen Natural Affinity Maturation Revealed by the Crystal Structure of Staphylococcal Enterotoxin G and its Binding to T-cell Receptor Vβ8.2

Marisa M. Fernández,[1,2†] Suparna Bhattacharya,[2†] Mauricio C. De Marzi,[1] Patrick H. Brown,[2] Melissa Kerzic,[2] Peter Schuck,[3] Roy A. Mariuzza,[2] and Emilio L. Malchiodi[1,2*]

[1]*Cátedra de Inmunología and Instituto de Estudios de la Inmunidad Humoral (IDEHU), Laboratorio de Inmunología Estructural, CONICET, Facultad de Farmacia y Bioquímica, Universidad de Buenos Aires, Buenos Aires, Argentina*

[2]*Center for Advanced Research in Biotechnology, W. M. Keck Laboratory for Structural Biology, University of Maryland Biotechnology Institute, Rockville, Maryland*

[3]*Division of Bioengineering and Physical Science, ORS, OD, National Institutes of Health, Bethesda, Maryland*

ABSTRACT **The illnesses associated with bacterial superantigens (SAgs) such as food poisoning and toxic shock syndrome, as well as the emerging threat of purpura fulminans and community-associated methicillin-resistant *S. aureus* producer of SAgs, emphasize the importance of a better characterization of SAg binding to their natural ligands, which would allow the development of drugs or biological reagents able to neutralize their action. SAgs are toxins that bind major histocompatibility complex class II molecules (MHC-II) and T-cell receptors (TCR), in a nonconventional manner, inducing T-cell activation that leads to production of cytokines such as tumor necrosis factor and interleukin-2, which may result in acute toxic shock. Previously, we cloned and expressed a new natural variant of staphylococcal enterotoxin G (SEG) and evaluated its ability to stimulate *in vivo* murine T-cell subpopulations. We found an early, strong, and widespread stimulation of mouse Vβ8.2 T-cells when compared with other SAgs member of the SEB subfamily. In search for the reason of the strong mitogenic potency, we determined the SEG crystal structure by X-ray crystallography to 2.2 Å resolution and analyzed SEG binding to mVβ8.2 and MHC-II. Calorimetry and SPR analysis showed that SEG has an affinity for mVβ8.2 40 to 100-fold higher than that reported for other members of SEB subfamily, and the highest reported for a wild type SAg-TCR couple. We also found that mutations introduced in mVβ8.2 to produce a high affinity mutant for other members of the SEB subfamily do not greatly affect binding to SEG. Crystallographic analysis and docking into mVβ8.2 in complex with SEB, SEC3, and SPEA showed that the deletions and substitution of key amino acids remodeled the putative surface of the mVβ8.2 binding site without affecting the binding to MHC-II. This results in a SAg with improved binding to its natural ligands, which may confer a possible evolutionary advantage for bacterial strains expressing SEG. Proteins 2007;68:389–402.** © 2007 Wiley-Liss, Inc.

Key words: bacterial superantigen; *Staphylococcus aureus*; SEG; T-cell receptor; MHC class II

INTRODUCTION

Superantigens (SAgs) are bacterial or viral toxins that bind major histocompatibility complex class II molecules (MHC-II) and T-cell receptors (TCR) in a nonconventional manner, inducing T-cell activation that leads to production of cytokines, such as TNF-α and IL-1β, and of T-cell mediators such as IL-2 and IFN-γ.[1–4] The high systemic levels of these interleukins and mediators induced by SAgs may result in pathological conditions, which may include fever and acute toxic shock.

Streptococcus pyogenes, a major human pathogenic bacterium, and *Staphylococcus aureus*, the most common cause of food borne illness and toxic shock syndrome, produce a large family of structurally related toxins that include streptococcal pyrogenic exotoxins (SPEs), staphylococcal enterotoxins (SEs), and the toxic shock syndrome toxin-1 (TSST-1). The SAg family tree based on

Abbreviations: CDR, complementarity-determining region; *egc*, enterotoxin gene cluster; FR, framework region; HV, hypervariable region; ITC, isothermal titration calorimetry; mVβ8.2, mouse TCR β chain variable β8.2; RU, resonance unit; SAg, superantigen; SE, staphylococcal enterotoxin; SPE, streptococcal pyrogenic exotoxin; SPR, surface plasmon resonance; SSA, streptococcus superantigen A; TSST-1, toxic shock syndrome toxin-1.

Grant sponsor: UBA, CONICET; Grant sponsor: ANPCyT; Grant number: PICT 12216; Grant sponsor: National Institutes of Health; Grant number: AI36900.

†Marisa M. Fernández and Suparna Bhattacharya contributed equally to this work.

Patrick H. Brown's current address is Division of Bioengineering and Physical Science, ORS, OD, National Institutes of Health, Bethesda, Maryland 20892.

*Correspondence to: Emilio L. Malchiodi, Cátedra de Inmunología, Facultad de Farmacia y Bioquímica-UBA, Junín 956 4 to P, 1113 Buenos Aires, Argentina. E-mail: emalchio@ffyb.uba.ar

Received 27 July 2006; Revised 12 December 2006; Accepted 15 December 2006

Published online 10 April 2007 in Wiley InterScience (www.interscience.wiley.com). DOI: 10.1002/prot.21388

primary amino acid sequence homology can be divided into four groups or sub-families with TSST-1 as an outlier in an individual branch.[5,6] Three-dimensional structures are now known for several members of the SEB subfamily including staphylococcal superantigens SEB,[7,8] SEC2[9] and SEC3[10]; and streptococcal superantigens SSA[11] and SPEA.[12] The binding of SAgs of the SEB subfamily to MHC-II and to TCR has been characterized at the molecular level from the structures of various complexes.[10–17] SEB binds via one face of their N-terminal β-barrel to the invariant α-chain of human HLA-DR1 molecule, contacting residues from the first and third turns of the β-sheet and from the N-terminal portion of the α helix,[13] without contacting the displayed peptide. This HLA-DR1 binding site on SEB is referred to as the generic MHC-II α-chain binding site. The mouse TCR β chain variable β8.2 (mVβ8.2) binding site on SEB and SEC2-3 consists of residues in a cleft between the two domains flanked by the N-terminal helix on one side of the cleft and loops from the N-terminal β-barrel on the other. SEB and SEC2-3 interact predominantly with residues from the second complementarity-determining region (CDR2), the third framework region (FR3), and to a lesser extent, the fourth hypervariable region (HV4) of the TCR β chain. Recently, the structure of the complex SPEA-mVβ8.2 was solved showing that besides those regions, SPEA make additional intermolecular contacts with CDR1.[17]

The latest incorporations into SEB subfamily are staphylococcal enterotoxins G (SEG) and R (SER). SEG was identified by Munson et al.[18] and is included in an enterotoxin gene cluster (*egc*) with the SAgs SEL, SEM, SEI, and SEK.[19] SEG is a 233 residues long toxin, corresponding to a mature protein of 27,043 Da, that shares 41–46% amino acid identity with other members of the SEB subfamily (SSA 46%, SEB 45%, SPEA 43%, SEC2-3 42%, SEC1 41%). SEG and other SAg from the *egc* cluster have being implicated recently in toxic shock syndrome and scarlet fever associated with infecting *S. aureus* strains. These strains lack genes for the classical members of the pyrogenic toxin SAg that comprises genes *sea-see* and the *tsst-1*.[20] In addition, recent reports showed a higher frequency of *seg/sei* than the classical *sea-see* and *tsst-1* genes, in *S. aureus* isolated from several sources.[21,22]

We recently analyzed the *in vivo* selective expansion of a distinct mouse T-cell subpopulation and found that SEG stimulates T-cells carrying Vβ7 and Vβ9 TCRs. Surprisingly, we also found an earlier, stronger, and more widespread stimulation of mVβ8.2 T-cell compared with other members of the SEB subfamily, which reach a maximum at Day 2 instead of Day 4 or later, as in SEC3 or SEB, respectively.[23–25] Here, we have characterized SEG binding to mVβ8.2 by SPR and calorimetry. The K_D determined by SPR, 0.125 μ*M*, was in close agreement with the K_D determined by calorimetry, 0.270 μ*M*. These affinities are the highest reported for an interaction of a wild type SAg and a TCR. We analyzed SEG binding to a high affinity mutant of mVβ8.2, L2CM,[26] finding that the mutated residues responsible for the increased affinity for SEC3[27] and SSA are not able to greatly improve the affinity for SEG. We also found that mVβ8.2 cannot simultaneously bind both SAgs. The high resolution crystal structure of SEG allowed us to find structural support for the biophysical studies and the biological effects. We found that deletions in the sequence and mutations of hot spot residues are responsible for structural remodeling of the putative binding surface of mVβ8.2 that would be responsible for an affinity 40- to 100-fold higher. The substitutions and deletion do not affect the binding to MHC-II resulting, as a whole, in a natural affinity maturated SAg that binds its natural ligands with increased specificity and affinity producing strong *in vivo* effects that could represent an evolutionary skill for *S. aureus*.

MATERIAL AND METHODS

Reagents and Bacterial Strains

All chemicals were of analytical grade and purchased from Sigma (St. Louis, MO). Restriction enzymes, Taq DNA polymerase, T4 ligase, and buffers for cloning were purchased from New England Biolabs (Beverly, MA). Ultra pure agarose was purchased from GIBCO BRL-Life Technologies (Rockville, MD).

Escherichia coli, DH5α and BL21 (DE3) strains where from Stratagene, La Jolla, CA. *E. coli* strains were grown in Luria-Bertani broth (LB) medium at 30°C or 37°C. Plasmid DNA was obtained by the alkaline lysis procedure using Qiagen Gel Extraction Kit.

Cloning Production and Purification of SAgs

seg gene (GenBank accession no ***AY961384***) obtained from the staphylococcal isolate Fc30 was cloned and expressed as described.[25] Briefly, *seg* 3′ terminal His_6-tagged was cloned between *Nco*I and *Bam*HI sites and expressed as a soluble protein in the bacterial periplasmic space. Soluble SEG was purified by addition onto a Ni^{2+}-nitrilotriacetic acid (Ni-NTA) column followed by Mono-S cation exchange column. The resulting protein preparation contained no others proteins as determined with a Coomassie blue-stained SDS-PAGE. Mass spectrometry and N-terminal sequencing established the identities of the recombinant protein.

Streptococcus superantigen A (SSA), staphylococcal enterotoxins C3 (SEC3) and I (SEI) were produced and purified as previously described.[28–30]

TCRs Production and Purification

Cloning of mouse TCR β chain Vβ8.2 (mVβ8.2mCβ1) and a high affinity mutant, LC2M, were previously described.[26] Briefly, mVβ8.2 and LC2M were cloned into the ampicillin resistant expression vector pT7-7 and expressed as inclusion bodies in *E. coli* BL21 (DE3). The inclusion bodies were washed and solubilized in 50 m*M* Tris-HCl pH 8.0, 8*M* urea, 2 m*M* EDTA, and 1 m*M* DTT. For *in vitro* folding, solubilized TCRs were diluted to a

final concentration of 20–50 μg/mL into 1*M* arginine, 50 m*M* Tris-HCl pH 8.5, 2 m*M* EDTA, 5 m*M* cysteamine, and 0.5 m*M* cystamine. After 3 days at 4°C, the folding mixture was concentrated, dialyzed against 50 m*M* Tris-HCl pH 8.5, and applied to a Mono Q anion exchange column (Amersham Biosciences) equilibrated in the same buffer. The protein was eluted with a linear NaCl gradient. Further purification was carried out by size exclusion using a Superdex 75 HR column (Amersham Biosciences) using PBS.

Expression and Purification of HLA-DR1

HLA-DR1 was produced by *in vitro* folding from bacterial inclusion bodies as described.[31] Briefly, plasmids encoding the HLA-DR1 α chain (DRA*0101) and β (DRB1*0101) chain were transformed separately into *E. coli* BL21(DE3) cells. Inclusion bodies were extensively washed and the subunits purified under denaturing and reducing conditions using an HQ50 anion exchange column (PerSeptive Biosystems). Purified subunits were diluted drop wise into a folding solution in the presence of 1 μ*M* HA peptide. Recombinant HA/HLA-DR1 was purified from the folding mixture using a Mono Q anion exchange column (Amersham Biosciences).

Affinity Assay

The interaction of soluble β chains with SAg was measured by SPR analysis using a Biacore 1000 instrument (Biacore, Piscataway, NJ), that allows determination of real time interactions between two molecules.[32] SAgs, mVβ8.2 or L2CM (~100 μg/mL) were dialyzed against 10 m*M* sodium acetate pH 5.5 and coupled to the carboxymethyl-dextran matrix of CM5 sensor chips (Biacore) using the Amine Coupling Kit as described.[33] The activation and immobilization periods were set between 3 and 7 min to couple the desired amount of proteins yielding between 260 and 1050 resonance units (RU). Micromolar concentrations of β chains mVβ8.2 and LC2M were dialyzed against Hepes-buffered saline (HBS) containing 150 m*M* NaCl and 0.005% surfactant P-20 (BIAcore). Twofold dilutions were made in the same buffer. All binding experiments were performed at 25°C. Dissociation was carried out in HBS. Pulses of 10 m*M* HCl were used to regenerate the surface. SEI, which does not bind mVβ8.2 or LC2M, and the β chain of human Vβ1, which does not react with member of SEB subfamily, were used as control. SPR data were analyzed using BIA-evaluation 4.1 software (Biacore). The dissociation constants (K_D) were determined by steady-state affinity analysis by measuring steady-state responses (after correction for nonspecific binding) at various concentrations, followed by nonlinear curve fitting analysis. Nonspecific binding was determined by passing ligand concentrations over surfaces with control protein immobilized.[34] All the experiments were repeated at least three times and the standard deviations were typically less than 12%. For interactions with measurable on- and off-rates, k_{on} and k_{off} were fitted simultaneously using a 1:1 (Langmuir) binding model, and K_D values were determined from the ratio k_{off}/k_{on}.

Analytical Ultracentrifugation

Sedimentation equilibrium studies were conducted in an Optima XL-I/A analytical ultracentrifuge (Beckman Coulter, Fullerton, CA) at a temperature of 4°C and at rotor speeds of 11,000 rpm, 17,000 rpm, and 21,000 rpm. One hundred and eighty microliters of protein was loaded into Epon double-sector centerpieces dissolved in phosphate buffered saline at concentrations of 20 μ*M* each, and in equimolar mixtures of 5, 10, and 20 μ*M*. Equilibrium profiles were acquired with the absorbance systems at wavelengths of 250 and 280 nm, and with the refractive index sensitive Rayleigh interference system. Protein buoyant molar masses and extinction coefficients were calculated from the analysis of the individual protein samples, using global multi-signal modeling of the sedimentation equilibrium profiles,[35] and using a specific interference optical signal increment of 3.3 fringes/(1.2 cm × mg/mL). They were found to be consistent with the expected values from amino acid composition, as determined with the software SEDNTERP. The mixtures were modeled with the well-known sedimentation equilibrium profiles of interacting species forming a reversible complex governed by mass action law. The analysis was performed with the software SEDPHAT (www.analyticalultracentrifugation.com), with implicit mass conservation constraints and algebraic noise decomposition,[35] and with the model being applied globally to all interference data at all rotor speeds and loading concentrations. Separately, an analogous global analysis was performed comprising all absorbance optical data, which gave consistent results, but at slightly lower discrimination of the complex.

Isothermal Titration Calorimetry

Calorimetric binding measurements were performed at 20°C using a Microcal VP-ITC titration calorimeter equipped with a 250 μL syringe rotating at 300 rpm (MicroCal, Northampton, MA). Concentrated protein stocks were dialyzed extensively against PBS (pH 7.5) and dilutions were prepared from filtered dialysis buffer. Experimental protein concentrations were determined spectrophotometrically using molar extinction coefficients of 14,770 M^{-1} cm^{-1} and 30,500 M^{-1} cm^{-1} for mVβ8.2 and SEG, respectively. The titration protocol entailed 1 × 5 μL injection followed by 28 × 10 μL injections of 400 μ*M* SEG into the calorimeter cell (1.4 mL volume) containing 30 μ*M* mVβ8.2. The raw calorimetric signal obtained for each injection was integrated and heats of binding were corrected for dilution of the titrant (SEG) by subtraction of the average heat associated with multiple injections of SEG performed after saturation of mVβ8.2. Nonlinear least squares analysis of the resulting binding data using a single-site binding model was performed to determine the equilibrium dissociation

TABLE I. Data Collection and Refinement Statistics for SEG

Data collection	
Space group	$P4_12_12$
Unit cell dimensions	
a (Å)	70.383
b (Å)	70.383
c (Å)	111.898
Resolution (Å)	33.7–2.2
Unique reflections[a]	15,065 (1475)
Completeness (%)[a]	99.9 (99.8)
R_{sym} (%)[ab]	7.2 (49.0)
Redundancy	26.4 (22.9)
Refinement	
R_{work} (%)[c]	23.1
R_{free} (%)[d]	25.8
Protein residues	233
Water molecules	54
Average B factors (Å^2)	
Protein main chain atoms	46.47
Protein side chain	47.5
Waters	43.55
RMS deviations	
Bond lengths(Å)	0.007
Bond angles (degree)	1.2
Ramachandran plot statistics	
Core (%)	90.4
Allowed (%)	7.6
Generous (%)	2.0

[a]Values in parentheses are statistics of the highest resolution shell for SEG (2.28–2.20Å).
[b]$R_{merge} = \Sigma\ I_j - \langle I \rangle\ /\ \Sigma\ I_j$, where I_j is the intensity of an individual reflection and is the average intensity of the reflection.
[c]$R_{work} = \Sigma\,||F_o| - \langle |F_c| \rangle| / \Sigma\,|F_o|$, where F_c is the calculated structure factor.
[d]R_{free} is as R_{work} but calculated for a randomly selected 10% of the reflection not included in the refinement.

constant, K_D, the binding enthalpy, ΔH°, and the stoichiometry of the interaction, n.

Crystallization and Data Collection

Crystallization trials of purified SEG were carried out in hanging drops at protein concentrations of 14 mg/mL. Crystals grew at 4°C in 25% PEG (w/v), 0.2 m*M* $(NH_4)_2SO_4$, and 100 m*M* sodium acetate (pH 5.2). For data collection, crystals were cryoprotected by brief soaking in mother liquor containing 15% (v/v) glycerol and flash-cooled in liquid nitrogen. X-ray diffraction data to 3 Å resolutions were recorded at home at 100 K using an R-axis IV++ image plate detector. Higher resolution data (2.2 Å) was collected on beam line X25 of the Brookhaven National Synchrotron Laboratory using a Quantum-4 charge-coupled device detector. The data was processed and scaled using DENZO/SCALEPACK[36] (Table I).

Structure Determination and Refinement

The structure of SEG was solved by molecular replacement using AMoRe.[37] The search model consisted of SEB (Protein Data Bank code 3SEB[8]). Only one SEG molecule could be found in molecular replacement, corresponding to a Matthews's coefficient of 2.77 (solvent content ~55%). The molecular replacement solution was refined with CNS 1.1[38] and the model was adjusted with XtalView[39] based on σ_A-weighted F_o–F_c and $2F_o$–F_c electron density maps. The quality of the model was checked with PROCHECK.[40] The refinement statistics are summarized in Table I. Atomic coordinates and structure factors have been deposited in the RCSB Protein Data Bank as entry **1XXG**.

RESULTS

Overall SEG Structure

The three-dimensional structure of SEG was determined at 2.2 Å resolution by X-ray crystallography using the SEB structure[8] as a search model. The initial model solution gave a correlation coefficient of 39.4% and R-factor of 48% at a resolution range of 10–4 Å. Refinement was carried out using CNS 1.1[38] including rigid body refinement, iterative cycle of simulated annealing, positional refinement, torsional angle refinement and group temperature (B) factor refinement, interspersed with model rebuilding into σ_A – weigthed F_o–F_c and $2F_o$–F_c electron density map using Xtal View.[39] Water molecules were added only to (F_o–F_c) density higher than 3σ and standard hydrogen bonding geometry. The final model consisted of 233 residues, 54 water molecules and one sulphate ion. The final R_{work} is 23.1% and R_{free} is 25.8% for all data between 33 and 2.2 Å (Table I). The quality of the protein structure was assessed by the program PROCHECK.[40] In the Ramachandran plot, 90.4% of the residues are found in the preferred region with no residues lying in the disallowed region (Table I).

The structure of SEG conforms to the generic bacterial SAgs comprising an N-terminal β-barrel domain (OB-fold) and a C-terminal β-grasp domain with β sheets that wrap around a long α-helix (Fig. 1). The β6-β7 disulphide loop was disordered and the residues from Asp99 to Asn103 could not be located; Glu121 could not be visualized either. Otherwise, the overall electron density for the structure was well defined. SEG has structural similarities to other members of the SEB subfamily and indeed, a structural alignment of Cα atoms of SEG versus SEB, SSA, and SEC3 reveals an r.m.s deviation

Fig. 2. Superantigens member of the SEB subfamily. (**a**) Structure-based alignment. Secondary structure elements for SEG (top) and SEC3 (bottom) are denoted by squiggles [α helices and 310 helices (η)] and arrows (β strands); these are numbered according to their order of appearance in the sequences. Residues that are invariant across SEB subfamily are shown in white on red background and those strongly conserved are shown in red. The remaining residues are in black. Secondary structural elements for SEG and SEC3 are indicated above and below the sequences, respectively. Key residues in mVβ8.2 binding that are replaced in SEG are indicated with black triangles. (**b**) Dendogram based on multiple SAg structure alignment. N-J Tree derived from multiple structural alignment of the SAgs. Sequence alignment and dendogram were performed with CLUSTALW (http://clustalw.genome.jp) and Fig. 2(a) was generated with ESPRIPT (http://espript.ibcp.sr/ESPript/ ESPript).

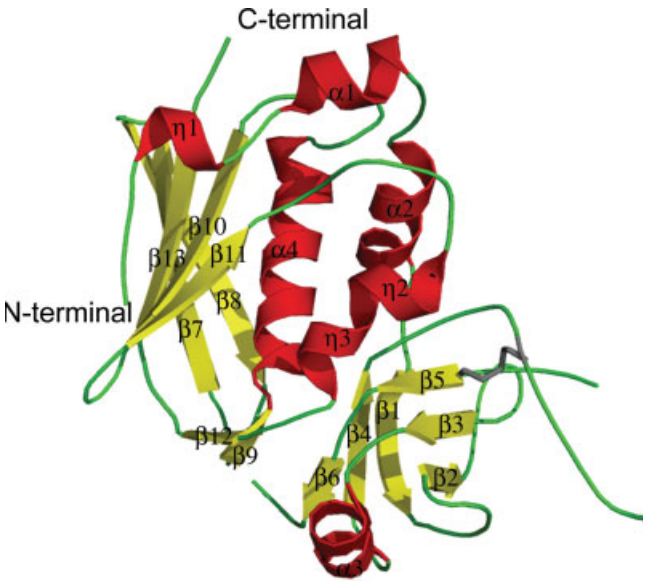

Fig. 1. Structural representation of SEG. Ribbon diagram showing the secondary structure elements in SEG, α-helix are in red, β sheets are in yellow, loops are in green and disulfide bridge is shown in ball-and-stick representation. Figure was drawn with MOLSCRIPT[41] and rendered with RASTER 3D.[42]

of around 1.2 Å, despite only 41–46% sequence identity. A structure-based sequence alignment of SEG with SEB, SSA, SPEA, and SEC1-3 [Fig. 2(a)], shows differences which comprise the β2-β3 loop and the interdomain loop between β6-β7, in both cases due to deletion of three amino acids in SEG, and a disruption in SEG α5 helix which is absent in the other SAgs of SEB subfamily. These differences and the change in key residues could have an impact on the affinity and binding mode to a TCR, as discussed below.

SEG Binding to mVβ8.2 TCR is Characterized by an Affinity in the Nanomolar Range

Several members of SEB subfamily are known to interact with mVβ8.2. The crystal structures of mVβ8.2 in complex with SEB, SEC2-3, or SPEA have been reported and extensive analysis both in structural terms, as well as by alanine-scanning mutagenesis, identified hot spots in SAg binding to mVβ8.2.[43] Sequence alignment of the SEB subfamily reveals that SEG presents changes in three highly conserved key amino acid positions, Asn58, Tyr88, and Gln206 (SEG numbering),

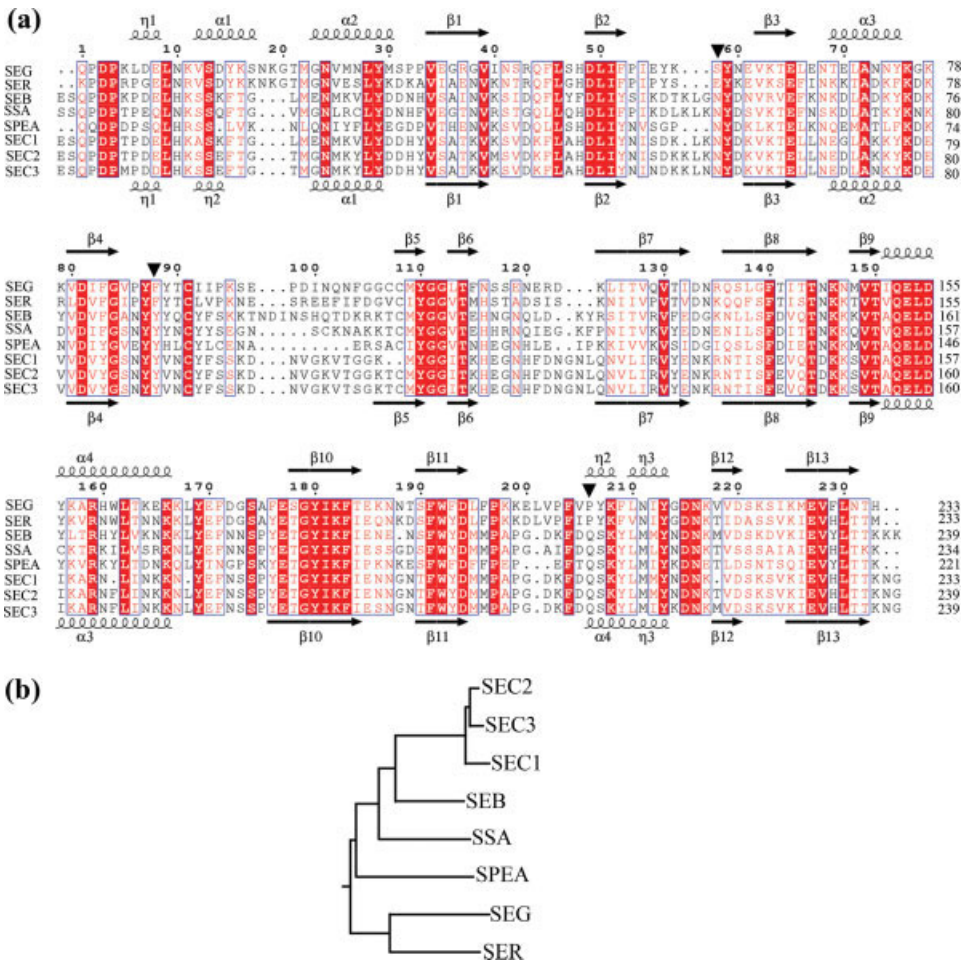

Figure 2.

which has been replaced by Ser58, Phe88, and Pro206, respectively [Fig. 2(a)].

Recently, we analyzed the *in vivo* stimulation of the mouse T-cell repertoire by SEG, finding it indeed stimulates mVβ8.2. Surprisingly, the stimulation of these particular T-cells was earlier and stronger compared with SEC3 and other members of the SEB subfamily.[25] To investigate the relationship between the affinity of SEG for mVβ8.2 and its ability to activate T-cell carrying this TCR, we analyzed the interaction of recombinant mVβ8.2 with SEG by surface plasmon resonance (SPR). In a typical experiment, SEG was coupled directly to the dextran matrix through primary amino groups of the protein. Injections of different concentrations of mVβ8.2 over SEG gave specific binding, calculated as the difference between the total response and the nonspecific response determined over a surface with SEI immobilized [Fig. 3(a)]. The corresponding steady-state affinity analysis is shown in Figure 3(c) and the aparent K_D value of this interaction was determined to be 0.125 μ*M*. Efforts to examine the binding with mVβ8.2 immobilized on the sensor surface and SEB, SEC1-3, or SSA in solution were carried out by several authors without success.[4,25,26,28,34] This phenomenon could be related to the occlusion of the SAg binding site onto the surface of the β chain as a consequence of the immobilization process. Surprisingly, when soluble SEG was injected over 310 RU of mVβ8.2 directly immobilized on the dextran matrix, we observed specific binding in a concentration-dependent manner [Fig. 3(b)]. Nonlinear analysis gave a K_D of 0.39 μ*M* [Fig. 3(d)]. To analyze whether the binding of SEG to immobilized mVβ8.2 was a particular behavior of our β chain preparation, we analyzed the binding of other SAgs over the same surface with mVβ8.2 immobilized. Injections of SEC3 and SSA over immobilized mVβ8.2 showed a concentration-dependent binding that cannot be distinguished from the profile obtained over a control surface (not shown). A possible explanation for the binding of SEG to immobilized mVβ8.2 could be that SEG and SEC3 binding site on mVβ8.2 surface are different and the immobilization process exposes residues only involved in SEG binding.

The affinity between SEG and mVβ8.2 is the highest reported for a wild type SAg and a TCR including all the members of the SEB subfamily interacting with mVβ8.2, whose affinities are in the micromolar range. The strong binding of SEG to mVβ8.2 and the possibility that the affinity would be influenced somehow by the immobilization process in the SPR experiment, prompted us to analyze the binding by isothermal titration calorimetry (ITC), where both molecules are free in solution. Figure 4 shows the raw ITC profile obtained from a titration which involved 1 × 5 μL injection followed by 28 × 10 μL injections of a concentrated SEG stock into the calorimeter cell containing mVβ8.2 in PBS at 20°C. A binding isotherm was generated upon integration of the calorimetric signal and the curve was produced from the best-fit parameters resulting from a nonlinear least squares analysis of the data to a single site binding model. The equilibrium dissociation constant determined for the mVβ8.2-SEG interaction is 0.27 (±0.03) μ*M*; a value in excellent agreement with what was calculated from data obtained using SPR methods (0.26 μ*M* as an average). The stoichiometry of the interaction is 1 mVβ8.2 to 1 SEG molecule. The Gibbs free energy change for the formation of the mVβ8.2-SEG complex (−8.80 kcal/mol) is comprised of favorable contributions from both the enthalpy and entropy terms with $\Delta H^\circ = -7.15$ kcal/mol, and $T\Delta S^\circ = 1.65$ kcal/mol.

SEG Binds a High Affinity Mutant of mVβ8.2 With Similar Affinity Than the Wild Type

L2CM is a variant of the murine T-cell receptor Vβ8.2 derived from yeast display mutagenesis with up to 1500-fold increased affinity for the SAg SEC3.[26] The higher affinity SEG displays for mVβ8.2 compared with SEC3 prompted us to analyze the binding of SEG to L2CM. We first analyzed whether the higher affinity of L2CM was a phenomenon restricted to SEC3, or whether it can be observed with other members of SEB subfamily. For that purpose, we analyzed mVβ8.2 binding to immobilized streptococcus superantigen A (SSA) finding a K_D = 101 μ*M* [Fig. 5(a,c)], which is in the range of affinities with other members of SEB subfamily (SEB, 144; SEC1, 19.8; SEC2, 7.9; SEC3, 7.5 and SPEA, 6.2 μM).[26,34] When different concentrations of L2CM were passed over immobilized SSA [Fig. 5(b,d)], we found a much higher affinity with K_D = 0.301 μ*M*, mostly due to a slower dissociation rate, as was previously observed with SEC3.[26] In contrast, when different concentrations of L2CM were passed over immobilized SEG a kinetic analysis yield a K_D = 0.034 μ*M* [Fig. 6(a)] and the nonlinear analysis indicate a K_D = 0.047 μ*M* [Fig. 6(b)], in both analysis a small increase in affinity to what was obtained for the wild type mVβ8.2 (K_D = 0.125 μ*M*), mostly due to a slower dissociation rate. Compared with mVβ8.2, L2CM shows affinities 1500 and 336 times higher for SEC3 and SSA, respectively, whereas only a 2.6-fold increase in affinity is displayed for SEG when steady-state affinity analyses are considered (Table II). These results suggest that the mutated residues in L2CM that produce increased affinity for SEC3[27] and SSA are not able to greatly improve the affinity for SEG.

Can SEC3 and SEG Simultaneously Bind to mVβ8.2?

The changes in three residues highly conserved among the SAg that bind mVβ8.2, the strong binding affinity determined for SEG-mVβ8.2 interaction, the unexpected binding to immobilized mVβ8.2, and the low increase in the affinity for the mutant L2CM, raised the possibility that the mVβ8.2 binding site on SEG might be different than the expected and that one molecule of mVβ8.2 would be able to accommodate two different SAgs. To address whether SEG and SEC3 can simultaneously bind to mVβ8.2, SPR and gel filtration experiments were conducted. In our own experience, SAg-TCR complexes

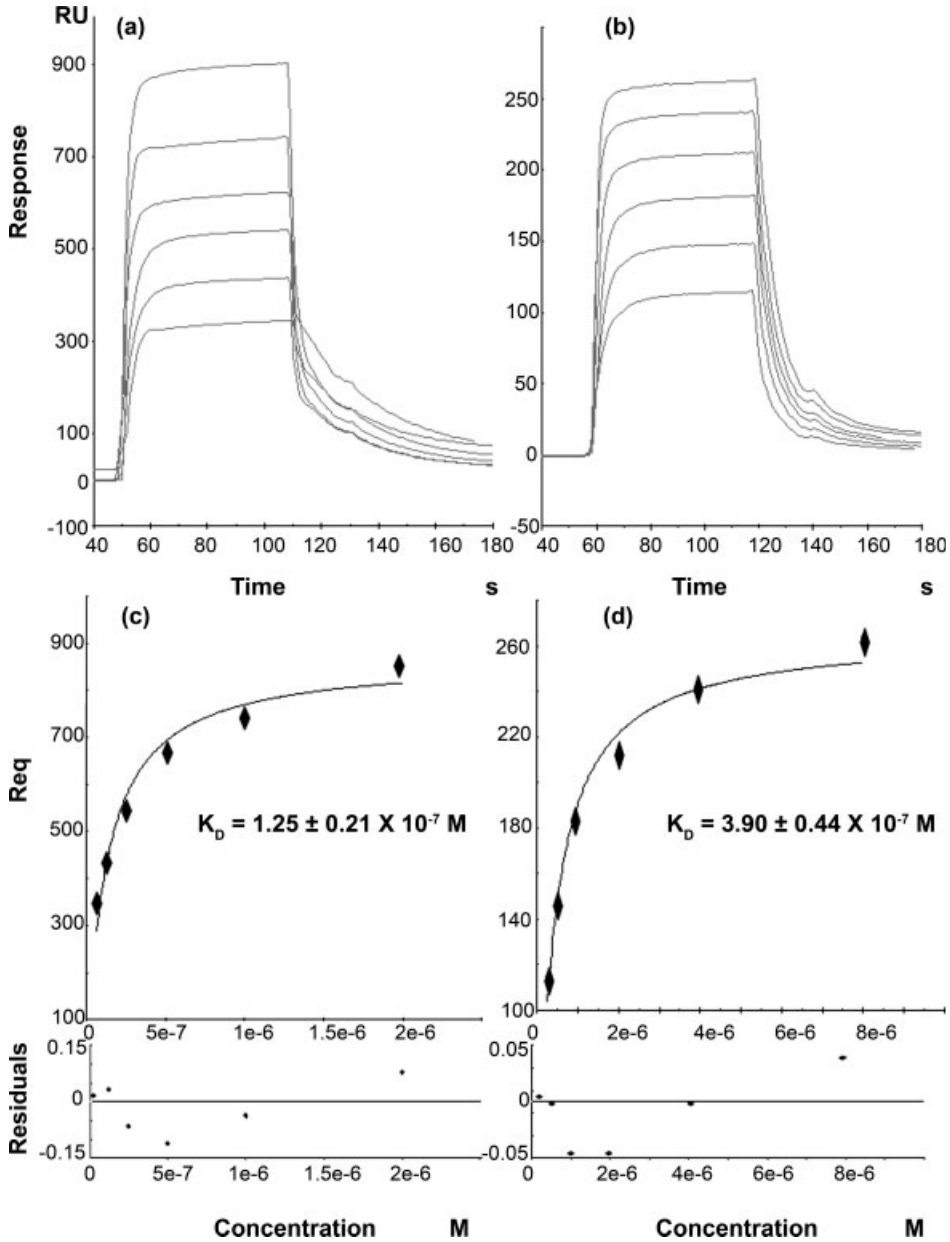

Fig. 3. SEG-mVβ8.2 Surface Plasmon Resonance Analysis. SPR sensorgrams of the interactions between mVβ8.2 (58–1875 η*M*) (**a**) and SEG (250–8000 η*M*) (**b**) with immobilized SEG (980 RU) (a) or mVβ8.2 (310 RU) (b) after correction for nonspecific binding. Panels **c** and **d** show non-linear steady-state affinity analysis for panels a and b, respectively, with the residuals plot shown below. The apparent KD for the binding of mVβ8.2 to immobilized SEG was 0.125 μ*M*, and in the reverse orientation was 0.390 μ*M*.

having affinities of 10 μ*M* or higher could usually be purified as a single species by gel filtration. Considering the high affinities involved, in the case that mVβ8.2 can simultaneously accommodate both SEG and SEC3, the molecules would elute as a trimolecular complex. On a previously calibrated Superdex S-200 column, we loaded highly purified mVβ8.2, SEG, SEC3, mixtures containing equimolar quantities of mVβ8.2 and SEG or mVβ8.2 and SEC3, and a mixture of the three proteins in 2:1:1 molar ratio, respectively. Figure 7(a) shows that when the three proteins are loaded on the column, a profile with two peaks containing either mVβ8.2-SEG or mVβ8.2-SEC3, representing ~50% of each bimolecular complex, was obtained. No peak was observed at ~14 mL, as would be expected for the formation of a trimolecular complex. The inability of mVβ8.2 to simultaneously accommodate the two SAgs was corroborated by SPR. We employed the high affinity mutant L2CM in order to obtain a slower dissociation rate which would allow the binding of the second SAg while the β chain is still bound to the immobilized SAg. Thus, SEG or SEC3 were immobilized on CM5 chip and L2CM was passed over

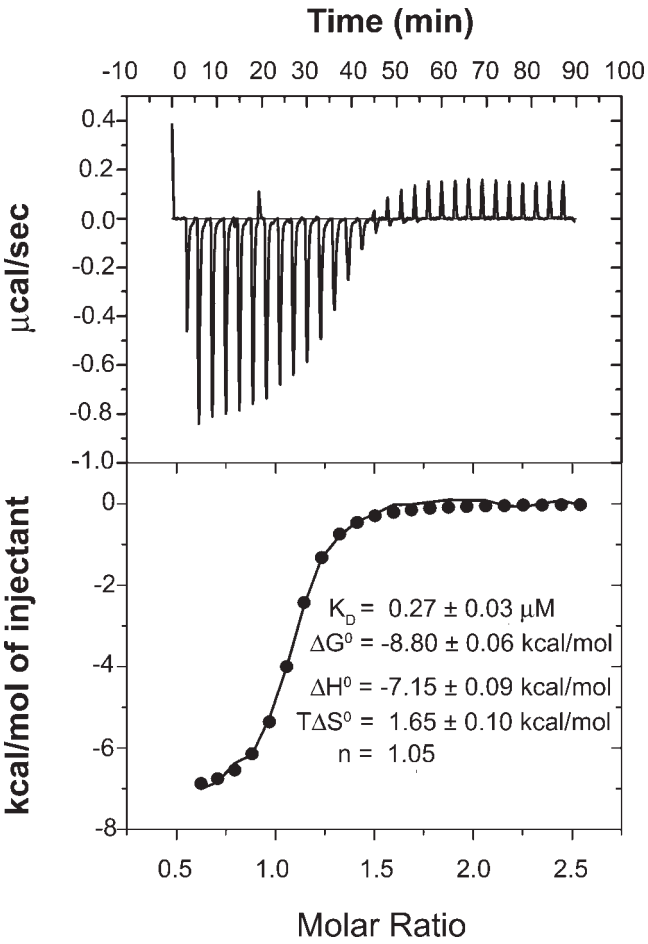

Fig. 4. Calorimetric titration of mVβ8.2 with SEG. The titration protocol involved 1 × 5 μL injection followed by 28 × 10 μL injections of SEG (400 μ*M*) into the calorimeter cell containing mVβ8.2 (30 μ*M*) in PBS (pH 7.5) at 20°C. Production of heat during the titration of mVβ8.2 with SEG (upper panel) and integrated data (lower panel) are shown. The thermodynamic parameters governing the interaction are shown in the lower panel.

the surface. SEG or SEC3 were injected in the dissociation phase. The staphylococcal SAg SEI, which does not bind mVβ8.2, was also injected at the same concentration. Figure 7(b) shows the increase in RU when SEG, SEC3, or SEI were injected, reflecting the bulk of the protein concentration. The expected specific increase in RU in the case of a second SAg molecule bound to the immobilized complex SAg-β chain was not observed in either case. Taken together, these results show that the binding site of SEG and SEC3 overlap on mVβ8.2, or are close enough that steric hindrance prevents the simultaneous binding of both SAgs.

SEG Binds HLA-DR1 More Tightly Than SEC3

To address whether the surprisingly strong mitogenic potency of SEG relative to other SAgs members of the SEB subfamily could be attributed to tighter binding to MHC class II on antigen presenting cells, we examined the binding of SEG to soluble recombinant HLA-DR1 loaded with HA306-318 by sedimentation equilibrium. The amino acid sequence and structural analysis of SEG support a SEB-like interaction with the α chain of MHC-II[13] since the most important residues of SEB that contact DR1 molcule are conserved. Thus, residues Gln44, Phe45, Leu46, Tyr87, and Tyr110 (SEG numbering) that make hydrogen bond contacts are conserved in SEG. In addition, most of the hydrophobic residues stabilizing the SEB-DR1 interaction, Phe45, Leu46, and Phe48, are present in SEG, or conservatively substituted. The salt bridge provided for Glu65 with the surrounding residues Y87 and Y110 that make H-bonds are strictly conserved [Fig. 2(a)], and other key contact residues as Lys76 and Lys208 are also conserved. Before analysis of the equilibrium constant for DR1 binding to SEG, the behavior of the individual MHC-II molecule and SAg was evaluated in separate sedimentation experiments. Both species were well behaved, showing virtually no tendency to aggregate at concentrations up to ~25 μ*M*. An estimate for the molecular weight of the DR1 was 45,000 Da, in good agreement with that expected from its amino acid composition (45,600). The molecular weight of SEG was determined to be 28,300 Da compared with an expected value of 28,700. The equilibrium dissociation constant determined by sedimentation equilibrium for DR1 with SEG was estimated at 32 μ*M* (Fig. 8), which is a lower affinity than that previously reported for SEB (14 μ*M*), but higher than for SEC3 (48 μ*M*).[40] Therefore, the higher superantigenic activity of SEG relative to SEC3 can be at least partially explained by the tighter binding of SEG to MHC class II.

DISCUSSION

Studies of SEG have been conducted showing this SAg could be involved in menstrual and nonmenstrual TSS or staphylococcal scarlet fever in *S. aureus* strains that produced none of the SAgs known to be involved in these syndromes.[20] On the basis of sequence homology, SEG has been included as a member of the SEB subfamily, the members of which are known to interact with mVβ8.2 TCR. Sequence alignment of SEG with SEB, SSA, SPEA, and SEC1-3 shows that SEG presents substitutions in three key residues located in the putative binding surface for mVβ8.2, which are conserved among the members of the subfamily. Recently, in studies comparing the specificity and mitogenic potency of SAgs, we found that SEG has characteristics that distinguish it from other members of the SEB subfamily.[25] Thus, inoculation of SEG into the right hind footpad of AKR/J mice showed: (1) stimulation of T-cells carrying mVβ8.2 with a maximum at Day 2 after inoculation, instead of Day 4, as expected; (2) the proliferation of mVβ8.2 T-cells in lymph nodes of mice inoculated with SEG was twice as great as in mice inoculated with SEC3; and (3) the stimulation effect is not only in the lymph node from the inoculated leg but also in the lymph node from the left hind inoculated with PBS, indicating a widespread effect.[25] This earlier and stronger stimulation was induced only

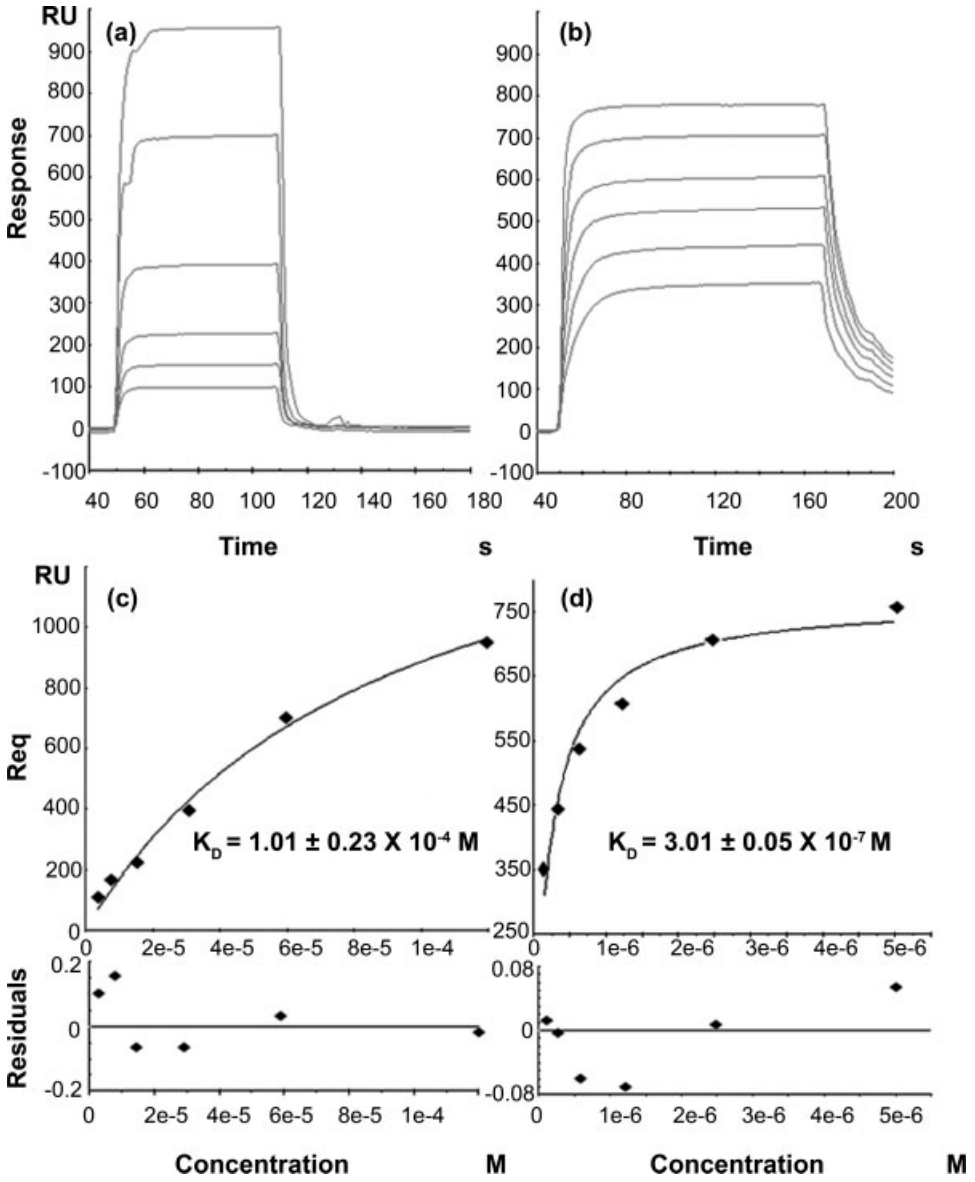

Fig. 5. Equilibrium binding of mVβ8.2 to SSA. SPR sensorgrams of the interactions between mVβ8.2 (3.75–120 μ*M*) (**a**) and high affinity mutant L2CM (150–5000 η*M*) (**b**) with immobilized SSA (1050 RU) after correction for nonspecific binding. Panels **c** and **d** show nonlinear steady-state affinity analysis for panels a and b, respectively, with the residuals plot shown below. The apparent KD for the interactions mVβ8.2-SSA and L2CM-SSA were 101 and 0.301 μ*M*, respectively.

in T-cells bearing mVβ8.2, but not in T-cells bearing mVβ7 and mVβ9, which are also stimulated by SEG, suggesting a unique interaction mode between SEG and mVβ8.2. Since mVβ8.2 was described as the principal TCR involved in experimental autoimmune encephalitis and taking into account the suggested role of SAgs in autoimmune diseases,[44,45] it is important to analyze the binding of SAgs that stimulate T-cells carrying this particular β chain.

With the aim of characterizing the interaction between SEG and mVβ8.2, we analyzed the binding by SPR. When we immobilized SEG on the sensor chip, we found a K_D = 0.125 μ*M*, which is 40- to 100-fold higher than that reported for other members of SEB subfamily and the highest reported for a wild type SAg-TCR couple. SAg-TCR interactions are usually characterized by affinities in the range of 5–150 μ*M*, remarkably similar to TCR-peptide-MHC interactions. On the contrary, the K_D determined for SEG-mVβ8.2 is in the range of the K_D reported for antibody–antigen interactions, whose affinities are typically in the nanomolar range and have a higher specificity when compared to TCR-peptide-MHC recognition.[46] The high affinity of this complex was confirmed by calorimetry, where both interacting species are in solution. In addition, SPR analysis of SEG binding to L2CM, a high affinity mutant of mVβ8.2 which displays

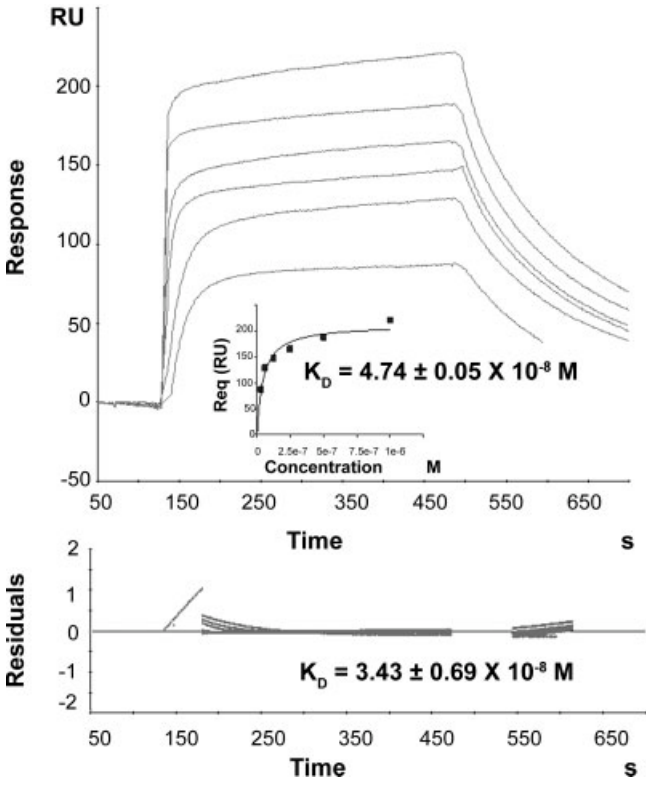

Fig. 6. Kinetic and equilibrium analysis of L2CM binding to SEG. SPR sensorgram of two fold dilutions of L2CM (31–1000 ηM) binding to immobilized SEG (260 RU) after correction for nonspecific binding. Global fitting of data to 1:1 binding model was done between 140 and 620 s and the corresponding residuals values are plotted below the sensorgram. Inset: non-linear steady-state affinity analysis of the specific binding of L2CM to immobilized SEG. The K_D value obtained by kinetic analysis (0.034 μM) is in closed agreement with the K_D derived from the steady-state analysis (0.047 μM).

TABLE II. Binding Affinities (μM), Obtained by SPR,[a] of SAgs of the SEB Subfamily for mVβ8.2 and Mutant L2CM

	Analyte		
Immobilized	mVβ8.2	L2CM	Affinity increase
SEC3[26]	7.5	0.005	1500
SSA	101	0.301	336
SEG	0.125	0.047	2.6

[a]For comparison purposes, K_D values are those obtained in equilibrium binding from nonlinear curve fitting analysis.

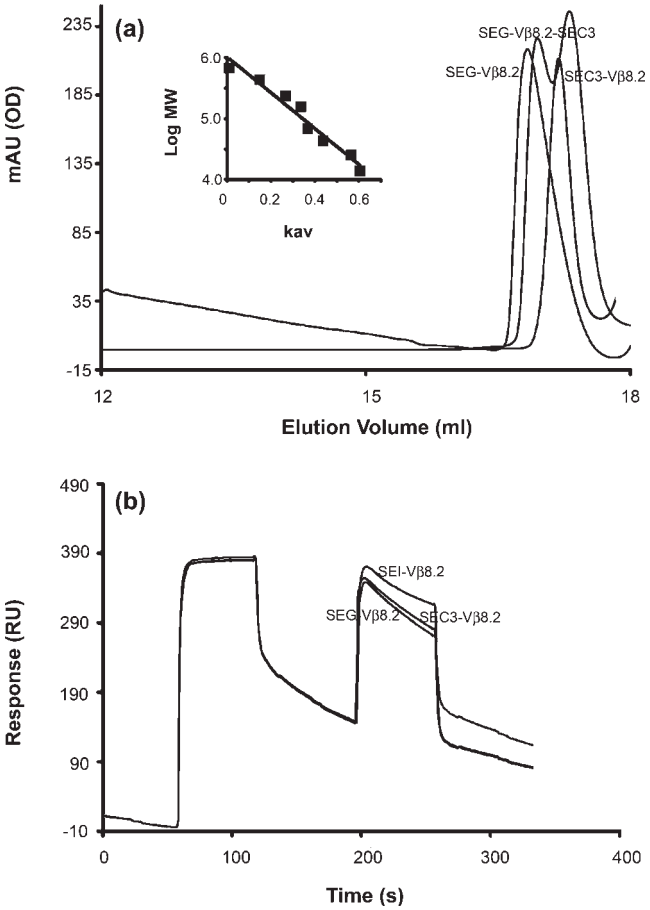

Fig. 7. Analysis of mVβ8.2 capacity to accommodate two SAgs. (**a**) S200 profile of mVβ8.2 in complex with SEG or SEC-3. Size exclusion chromatogram of mixtures containing equimolar quantities of mVβ8.2 and SEG or mVβ8.2 and SEC3, and mVβ8.2, SEG and SEC3 in a 2:1:1 molar ratio; loaded on a Superdex 200 HR column and monitored by absorbance at 280 nm. The column was previously calibrated with thiroglobulin, ferritin, catalase, aldolase, BSA, OVA, chymotrypsinogen A, and ribonuclease A as m.w. standards; the void volume was determined using blue dextran 2000 (inset). (**b**) SPR analysis of the interaction of L2CM with SEG and SEC3. SEC3 was immobilized on the dextran matrix and 20 μM L2CM was passed for 100 s. Buffer flow rates were 5 μL/min. Equilibrium binding levels were reached within 10 s. In the dissociation phase with HBS, 20 μM of SEC3, SEG, or SEI was injected and the increase in RU was recorded. No significant differences were observed when any of the three SAgs were injected.

as much as 1500 times higher affinity for member of the SEB subfamily,[26] showed a small increase in the affinity over the wild type mVβ8.2. An explanation for a lesser increase could be that the binding of SEG to mVβ8.2 is already optimized and the mutations in L2CM lead only to a small improvement in affinities, or other residues from mVβ8.2 and L2CM, besides the ones that constitute the known structural epitope, are also contacting residues for SEG. Previous studies[26,27] assessed the energetic consequences of the mutations introduced in wild-type mVβ8.2 and revealed that four of the mutated residues in L2CM are energetically significant in terms of improved binding to SEC3, and can readily explain why L2CM affinity for SEG is 10-fold lower than for SEC3 (Table II). These residues constitute the functional epitope that is responsible for the increased affinity of L2CM and include the A52V$^{V\beta}$, S54N$^{V\beta}$, K66E$^{V\beta}$, and Q72H$^{V\beta}$ mutations. The variant A52V$^{V\beta}$ increases the buried hydrophobic surface area with residue Tyr88 from SEC3 (SEG numbering), which is a Phe88 in SEG and would be a conservative substitution for this contact [Fig. 2(a)]. The variant S54N$^{V\beta}$ facilitates an extensive water-mediated hydrogen bonding network with residues Asp202, Lys203, and Phe204 in SEC3. In SEG, Phe204 is conserved and Lys203 is substituted by Pro, however,

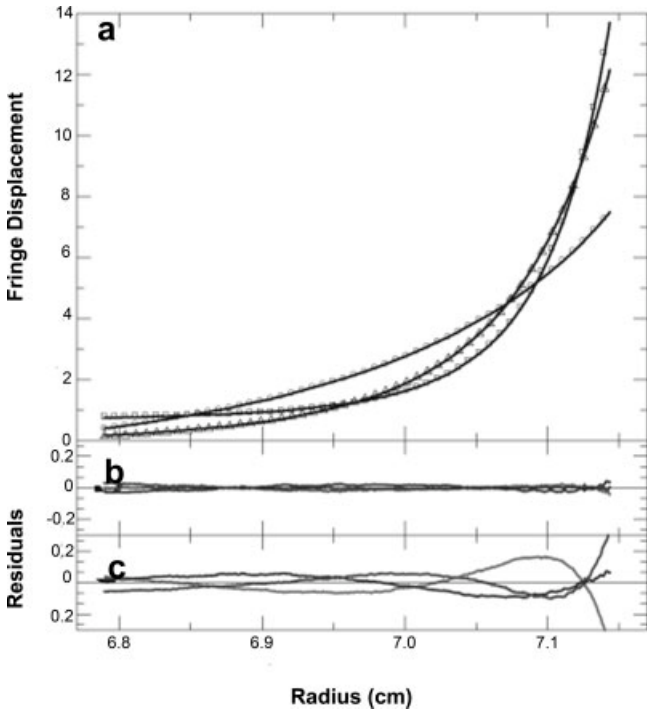

Fig. 8. Sedimentation equilibrium analysis of the interaction of DR1 with SEG. (**a**) Shown are interference optical fringe displacement distributions of an equimolar mixture of DR1 and SEG at rotor speeds of 11,000 rpm (circles), 17,000 rpm (triangles), and 21,000 rpm (squares) (only every 10th data point shown), which were analyzed as part of a global fit of similar data sets at three different loading concentrations (5, 10, and 20 μM). Solid lines are the global best-fit distributions using a reversible monomer-dimer model with an equilibrium constant of K_D = 32 μM. (**b**) Residuals of the fit, with an rms deviation to the data shown of 0.013 fringes. (**c**) For comparison, the residuals of the best-fit distributions are shown if the absence of an interaction was assumed, with an otherwise identical model.

the S54N$^{V\beta}$ hydrogen bonds are with main chain atoms and thus, expected to be conserved. Asp202 is substituted by Val202, which can cause disruption of the network of hydrogen bonds because the oxygen atom of the side chain of Asp202 is involved. K66E$^{V\beta}$ interacts with Phe171, which is conserved in SEG. The impact of Q72H$^{V\beta}$ is difficult to assess because it makes contacts with the disulfide loop in SEC3, which could not be resolved in the crystal structure of either SAg and it is not conserved [Fig. 2(a)].

It was previously shown that there is a clear and simple relationship between the affinity of SAgs for the TCR and their biological activity: the tighter the binding of a particular SAg to the TCR β chain, the greater its ability to stimulate T-cells.[47] It was also found that there is interplay between TCR-SAg and SAg-MHC interactions in determining mitogenic potency, such that a small increase in the affinity of a SAg for MHC can overcome a large decrease in the SAg's affinity for the TCR.[43] Since no affinities have been reported for the interaction of SAgs with mouse class II molecules, several authors have made a parallelism with human MHC-II, suggesting that weak interaction with TCR β chain could be compensated by sufficiently tight interaction with MHC-II. Thus, SEB on a molar basis is a toxin 3- to 10-fold more effective than SEC3 in stimulating the mouse parental 14.3 T-cell hybridoma, which expresses mVβ8.2.[34] SEB showed unexpectedly weak binding to mVβ8.2 (K_D = 144 μM) but tighter interaction with DR1 (K_D = 15 μM), compared with SEC3 (K_D = 7 μM for mVβ8.2; and K_D = 40 μM for DR1). Consequently, SEB's powerful superantigenicity was explained based on its tighter interaction with the MHC-II molecules. SEG not only exhibits an affinity 60-fold higher than SEC3 for mVβ8.2, while retaining a fast dissociation rate that could allow sequential binding to several molecules, but also has tight affinity for MHC (K_D = 32 μM), which might explain the earlier and stronger stimulation *in vivo* of T-cells bearing mVβ8.2.[25]

The high resolution crystal structure of SEG has allowed us to carry out a better characterization of the interaction between SEG and mVβ8.2, finding structural support for the biophysical studies described above. Crystal structures of mVβ8.2 in complex with SEB, SEC2-3, or SPEA have been reported[10,15,17] and extensive analysis both in structural terms as well as from alanine-scanning mutagenesis studies have established the relative energetic contribution of the residues involved in the binding of these SAg to mVβ8.2.[44] The mVβ8.2 binding surfaces of SEB, SEC3, and SPEA, as determined by X-ray crystallography of the complexes, and SSA's putative binding surface,[11] showed conservation of most of the eight contacting residues, the so-called functional epitope, which display a continuous surface in these SAgs (Fig. 9). Several of those residues have been identified as "hot spots" because of their energetic contribution to binding.[45] The SEG structure reveals differences in three of these hot spots, Asn58, Tyr88, and Gln206 (SEG numbering), which have being replaced by Ser58, Phe88, and Pro206, respectively; moreover, the surface displayed by the eight residues is no longer continuous. Instead, SEG presents residues Tyr59, Pro203, and Phe204 on the surface facing mVβ8.2, (Fig. 9, inset), which might result in a greater binding affinity.

In search for the reason of a particular binding mode between SEG and mVβ8.2, the refined structure of SEG was superposed onto SEB, SEC3, and SPEA in complex with mVβ8.2, to analyze the differences in the surface of the TCR binding region (Fig. 10). Crystal structures of mVβ8.2 in complex with SEB, SEC2-3, and SPEA showed that four hydrogen bonds are formed between mVβ8.2 backbone and side chain of residues from SAg in the TCR binding surface. Among SEB, SEC1-3, SPEA and SSA, all members of SEB subfamily that react with mVβ8.2, residues Asn24, Asn58 and Gln206 are strictly conserved and make hydrogen bonds with Tyr55, Pro70, and Gly53, respectively, on mVβ8.2 surface. In SEG, Asp58 has been substituted by serine, whose side chain is buried in the structure of SEG and oriented away from the mVβ8.2 binding surface due to a three-residue deletion in the β2-β3 loop where Ser58 is located (see Fig. 9). There is a difference in alpha helix α5, which is conserved in all the SAg of SEB subfamily that may be

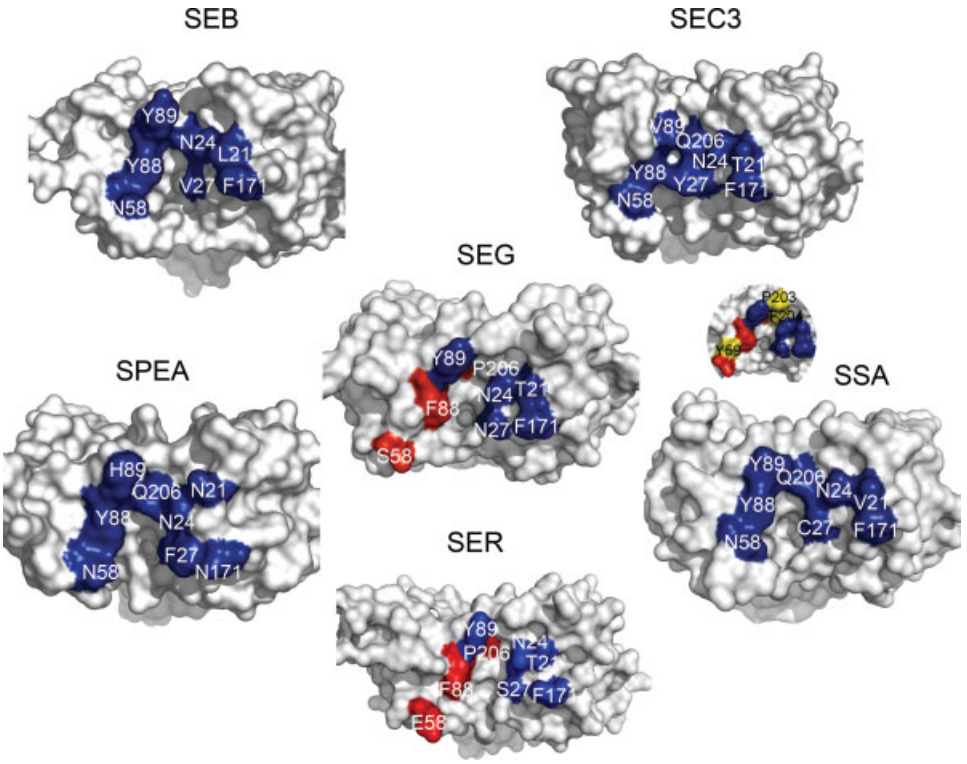

Fig. 9. Comparison of the mVβ8.2 TCR binding surface topology of SAgs of the SEB subfamily. SAgs are shown as molecular surface representations with only residues that are in contact (SEB, SEC3 and SPEA) or in the putative binding surface (SSA, SEG, and SER) with mVβ8.2 highlighted in colors. Residues in blue are highly conserved in members of SEB subfamily and display a continuous interaction surface in SEB, SEC3, SPEA, and SSA. Residues N58, Y88, and Q206 are strictly conserved in all the SAgs but in SEG and SER, where the replacing residues are shown in red. In yellow (inset) are the residues displayed in SEG surface that would be facing mVβ8.2. Figure was drawn with Pymol (Scientific LLC) and SER structure was modeled with Swiss Model (http://www.expasy.org/sprot).

due to the presence of a Pro206 in SEG, instead of Gln206, that could disrupt the binding site. The side chain of Pro206 is pulled away from the mVβ8.2 binding surface (Fig. 10) and the analysis of surface accessibility reveals that Pro206 in SEG is almost buried with a surface area of only 4.5 $Å^2$ compared to 22 $Å^2$ in SEB and SEC3, 25 $Å^2$ in SSA, and 30 $Å^2$ in SPEA (see also Fig. 9). Considering these differences and other characteristics of SEG binding such as: (1) the ability to interact with immobilized mVβ8.2 on the surface of the sensor chip, (2) the affinity for mVβ8.2 is not highly affected by the mutations in L2CM, and (3) the fact that we ruled out the possibility that SEG binding site on mVβ8.2 was located in some alternate spot to allow the accommodation of 2 SAg on the mVβ8.2 surface, it tempting to speculate that there are other residues from mVβ8.2 making contact with SEG "hot spots", or even other residues from SEG involved in the interaction with mVβ8.2, such as Tyr59, Pro203, and Phe204 that are on the surface of SEG facing mVβ8.2 (Fig. 9, inset). However, only a crystal structure determination of the SEG-mVβ8.2 complex will reveal the actual structural epitope.

Recently, a new SAg of *S. aureus*, SER, was discovered and included in the SEB subfamily based on sequence

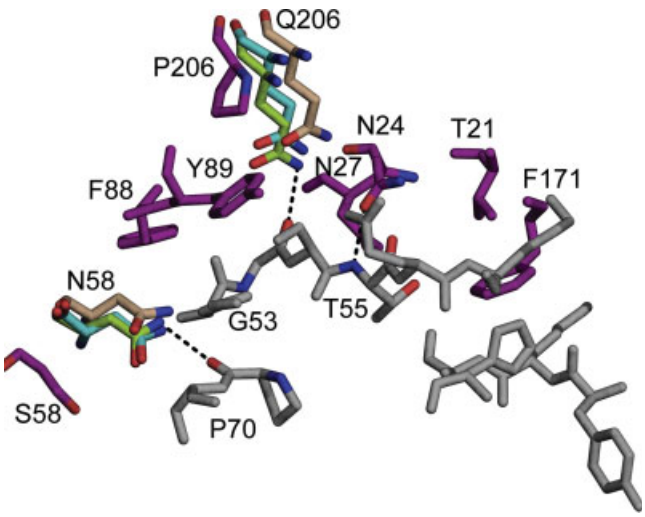

Fig. 10. Structure of SEG superimposed to the structure of SEC3, SEB and SPEA in complex with mVβ8.2. mVβ8.2 residues are in gray. SEG residues are in purple. Residues Q206 and N58 are green in SEB, blue in SEC3 and light orange in SPEA. Hydrogen bonds are represented by dotted lines. Distances were omitted for clarity.

homology.[48] Because SEG and SER share 60% amino acid identity, they may be grouped together in a different branch of the SEB subfamily [Fig. 2(b)]; the alignment shows that SER exhibits the same deletions in loops β2-β3 and β6-β7 as SEG [Fig. 2(a)]. In addition, SER shares with SEG the mutations Y88F and Q206P. Further, N58E is a conservative mutation, and the side chain of Glu58 in SER would be oriented away from the mVβ8.2 binding surface due to the three-residue deletion in the β2-β3 loop where it is located (Fig. 9). These characteristics allow us to predict that the interaction of SER with mVβ8.2 should be similar to the one described here for SEG.

SEG may be an example of natural affinity maturation process, by which proteins evolve to bind with increased specificity and affinity. The maturation through the binding of mVβ8.2 would include relatively minor changes with deletion and substitution in surface residues that conducted to a significant increase in the affinity. It seems that the structural remodeling of the molecular interface of SEG was intended for binding of mVβ8.2, the most abundant TCR β chain in mice, because stimulation of T-cells carrying Vβ7 and Vβ9 is indistinguishable from others. The increase in the affinity for mVβ8.2, while conserving its affinity for MHC class II molecules, might be a significant advantage for the strain that carries this SAg because it would increase the virulence and all virulent elements are considered as microbial evolutionary skills. The significance of this process gains increasing importance when taking into account the emerging threat of community-associated methicillin (formerly methicillin)-resistant *S. aureus*, that have being described as causing serious morbidity and even death in previously healthy children and adults, or the first cases of purpura fulminans, an acute illness recently associated with *S. aureus* strains that produce high levels of SAg.[49] Considering that illnesses associated with SAgs cannot be treated with antibiotics or standard procedures and the natural affinity maturation developed by pathogens may improve their evolutionary ability to avoid natural and artificial defense systems, it is important to conduct studies that contribute to a better characterization of SAg binding to their natural ligands. This, in turn, could facilitate development of drugs or biological reagents able to neutralize their action.

ACKNOWLEDGMENTS

The authors thank Howard Robinson for data collection at beamline X29 of the Brookhaven National Synchrotron Laboratory and Michael Murphy (Biacore) for invaluable advice.

REFERENCES

1. Fast DJ, Schlievert PM, Nelson RD. Toxic shock syndrome-associated staphylococcal and streptococcal pyrogenic toxins are potent inducers of tumor necrosis factor production. Infect Immun 1989;57:291–294.
2. Herman A, Kappler JW, Marrack P, Pullen AM. Superantigens: mechanism of T-cell stimulation and role in immune responses. Annu Rev Immunol 1991;9:745–772.
3. Hackett SP, Stevens DL. Streptococcal toxic shock syndrome: synthesis of tumor necrosis factor and interleukin-1 by monocytes stimulated with pyrogenic exotoxin A and streptolysin O. J Infect Dis 1992;165:879–885.
4. Seth A, Stern LJ, Ottenhoff TH, Engel I, Owen MJ, Lamb JR, Klausner RD, Wiley DC. Binary and ternary complexes between T-cell receptor, class II MHC and superantigen in vitro. Nature 1994;369:324–327.
5. Proft T, Arcus VL, Handley V, Baker EN, Fraser JD. Immunological and biochemical characterization of streptococcal pyrogenic exotoxins I and J (SPE-I and SPE-J) from *Streptococcus pyogenes*. J Immunol 2001;166:6711–6719.
6. Proft T, Fraser JD. Bacterial superantigens. Clin Exp Immunol 2003;133:299–306.
7. Swaminathan S, Furey W, Pletcher J, Sax M. Crystal structure of staphylococcal enterotoxin B, a superantigen. Nature 1992;359:801–806.
8. Papageorgiou AC, Tranter HS, Acharya KR. Crystal structure of microbial superantigen staphylococcal enterotoxin B at 1.5 Å resolution: implications for superantigen recognition by MHC class II molecules and T-cell receptors. J Mol Biol 1998;277:61–79.
9. Papageorgiou AC, Acharya KR, Shapiro R, Passalacqua EF, Brehm RD, Tranter HS. Crystal structure of the superantigen enterotoxin C2 from *Staphylococcus aureus* reveals a zinc-binding site. Structure (Camb) 1995;3:769–779.
10. Fields BA, Malchiodi EL, Li H, Ysern X, Stauffacher CV, Schlievert PM, Karjalainen K, Mariuzza RA. Crystal structure of a T-cell receptor β-chain complexed with a superantigen. Nature 1996;384:188–192.
11. Sundberg E, Jardetzky TS. Structural basis for HLA-DQ binding by the streptococcal superantigen SSA. Nat Struct Biol 1999;6:123–129.
12. Papageorgiou AC, Collins CM, Gutman DM, Kline JB, O'Brien SM, Tranter HS, Acharya KR. Structural basis for the recognition of superantigen streptococcal pyrogenic exotoxin A (SpeA1) by MHC class II molecules and T-cell receptors. EMBO J 1999;18:9–21.
13. Jardetzky TS, Brown JH, Gorga JC, Stern LJ, Urban RG, Chi YI, Stauffacher C, Strominger JL, Wiley DC. Three-dimensional structure of a human class II histocompatibility molecule complexed with superantigen. Nature 1994;368:711–718.
14. Kim J, Urban RG, Strominger JL, Wiley DC. Toxic shock syndrome toxin-1 complexed with a class II major histocompatibility molecule HLA-DR1. Science 1994;66:1870–1874.
15. Li H, Llera A, Tsuchiya D, Leder L, Ysern X, Schlievert PM, Karjalainen PM, Mariuzza RA. Three-dimensional structure of the complex between a T cell receptor β chain and the superantigen staphylococcal enterotoxin B. Immunity 1998;9:807–816.
16. Li Y, Li H, Dimasi N, McCormick JK, Martin R, Schuck P, Schlievert PM, Mariuzza RA. Crystal structure of a superantigen bound to the high-affinity, zinc-dependent site on MHC class II. Immunity 2001;14:93–104.
17. Sundberg EJ, Li H, Llera AS, McCormick JK, Tormo J, Schlievert PM, Karjalainen K, Mariuzza RA. Structures of two streptococcal superantigens bound to TCR β chains reveals diversity in the architecture of T cell signaling complexes. Structure (Camb) 2002;10:687–699.
18. Munson SH, Tremaine MT, Betley MJ, Welch RA. Identification and characterization of staphylococcal enterotoxin types G and I from *Staphylococcus aureus*. Infect Immun 1998;66:3337–3348.
19. Jarraud S, Peyrat MA, Lim A, Tristan A, Bes M, Mougel C, Etienne J, Vandenesch F, Bonneville M, Lina G. egc, a highly prevalent operon of enterotoxin gene, forms a putative nursery of superantigens in *Staphylococcus aureus*. J Immunol 2001;166:669–677. Erratum in: J Immunol 2001;166, following 4259.
20. Jarraud S, Cozon G, Vandenesch F, Bes M, Etienne J, Lina G. Involvement of enterotoxins G and I in staphylococcal toxic shock syndrome and staphylococcal scarlet fever. J Clin Microbiol 1999;37:2446–2449.
21. Becker K, Friedrich AW, Lubritz G, Weilert M, Peters G, Von Eiff C. Prevalence of genes encoding pyrogenic toxin superantigens and exfoliative toxins among strains of *Staphylococcus aur-*

eus isolated from blood and nasal specimens. J Clin Microbiol 2003;41:1434–1439.
22. Banks MC, Kamel NS, Zabriskie JB, Larone DH, Ursea D, Posnett DN. *Staphylococcus aureus* express unique superantigens depending on the tissue source. J Infect Dis 2003;187:77–86.
23. MacDonald HR, Baschieri S, Lees RK. Clonal expansion precedes anergy and death of Vβ8+ peripheral T-cells responding to staphylococcal enterotoxin B in vivo. Eur J Immunol 1991;21: 1963–1966.
24. Renno T, Attinger A, Locatelli S, Bakker T, Vacheron S, MacDonald HR. Cutting edge: apoptosis of superantigen-activated T-cells occurs preferentially after a discrete number of cell divisions in vivo. J Immunol 1999;162:6312–6315.
25. Fernández MM, De Marzi MC, Berguer P, Burzyn D, Langley R, Piazzon I, Mariuzza RA, Malchiodi EL. Binding of natural variants of staphylococcal superantigens SEG and SEI to TCR and MHC class II molecule. Mol Immunol 2006;43:927–938.
26. Yang J, Swaminathan CP, Huan Y, Guan R, Cho S, Kieke MC, Kranz DM, Mariuzza RA, Sundberg E. Dissecting cooperative and additive binding energetics in the affinity maturation pathway of a protein-protein interface. J Biol Chem 2003;278:50412–50421.
27. Cho S, Swaminathan CP, Yang J, Kerzic MC, Guan R, Kieke MC, Kranz DM, Mariuzza RA, Sundberg EJ. Structural basis of affinity maturation and intramolecular cooperativity in a protein-protein interaction. Structure (Camb) 2005;13:1775–1787.
28. De Marzi MC, Fernández MM, Sundberg EJ, Molinero L, Zwirner NZ, Llera AS, Mariuzza RA, Malchiodi EL. Cloning, expression and interaction of human T-cell receptors with the bacterial superantigen SSA. Eur J Biochem 2004;271:4075–4083.
29. Andersen PS, Lavoie PM, Sekaly RP, Churchill H, Kranz DM, Schlievert PM, Karjalainen K, Mariuzza RA. Role of the T cell receptor α chain in stabilizing TCR-superantigen-MHC class II complexes. Immunity 1999;10:473–483.
30. Fernández MM, Guan R, Swaminathan CP, Malchiodi EL, Mariuzza RA. Crystal structure of staphylococcal enterotoxin I (SEI) in complex with a human MHC class II molecule. J Biol Chem 2006;362:102–113.
31. Frayser M, Sato AK, Xu L, Stern LJ. Empty and peptide-loaded class II major histocompatibility complex proteins produced by expression in *Escherichia coli* and folding in vitro. Protein Expr Purif 1999;15:105–114.
32. Karlsson R, Michaelsson A, Mattsson L. Kinetic analysis of monoclonal antigen-antibody-antigen interactions with a new biosensor based analytical system. J Immunol Methods 1991;145: 229–240.
33. Johnsson B, Lofas S, Lindquist G. Immobilization of proteins to a carboxymethyldextran-modified gold surface for bioespecific interaction analysis in surface plasmon resonance sensors. Anal Biochem 1991;198:268–277.
34. Malchiodi EL, Eisenstein E, Fields BA, Ohlendorf DH, Schlievert PM, Karjalainen K, Mariuzza RA. Superantigen binding to a T cell receptor β chain of known three-dimensional structure. J Exp Med 1995;182:1833–1845.
35. Vistica J, Dam J, Balbo A, Yikilmaz E, Mariuzza RA, Rouault TA, Schuck P. Sedimentation equilibrium analysis of protein interactions with global implicit mass conservation constraints and systematic noise decomposition. Anal Biochem 2004;326: 234–256.
36. Otwinowski Z, Minor W.Processing of X-ray diffraction data collected in oscillation mode. In: Carter CW Jr, Sweet RM, editors. Methods in enzymology, Vol. 276: Macromolecular crystallography, Part A. New York: Academic Press; 1997. pp 307–326.
37. Navaza J. Implementation of molecular replacement in AMo Re. Acta Crystallogr D 2001;57:1367–1372.
38. Brünger AT, Adam PD, Clore G, DeLanod WL, Gros P, Grosse-Kunstleve RW, Jiang JS, Kuszewski J, Nilges M, Pannu NS, Read RJ, Rice LM, Simonson T, Warren GL. Crystallography and NMR system: a new software suite for macromolecular structure determination. Acta Crystallogr D 1998;54:905–921.
39. McRee DE. XtalView/Xfit. A versatile program for manipulating atomic coordinates and electron-density. J Struct Biol 1999;125: 156–165.
40. Laskowski RA, Moss DS, Thornton JM. Main-chain bond lengths and bond angles in protein structures. J Mol Biol 1993; 231:1049–1067.
41. Kraulis PJ. MOLSCRIPT. A program to produce both detailed and schematic plots of protein structures. J Appl Cryst 1991;24: 946–950.
42. Merritt EA, Murphy ME. Raster3D Version 2.0. A program for photorealistic molecular graphics. Acta Crystallogr D 1994;50: 869–873.
43. Leder L, Llera A, Lavoie PM, Lebedeva MI, Li H, Sekaly RP, Bohach GA, Gahr PJ, Schlievert PM, Karjalainen K, Mariuzza RA. A mutational analysis of the binding of staphylococcal enterotoxins B and C3 to the T cell receptor β chain and major histocompatibility complex class II. J Exp Med 1998;187:823–833.
44. Brocke S, Housmann B, Steimnman L, Wucherpfenning K. Microbial peptides and superantigens in the pathogenesis of autoimmune diseases of central nervous system. Sem Immunol 1998;10:57–67.
45. Madakamutil LT, Maricic I, Sercarz E, Kumar V. Regulatory T cells control autoimmunity in vivo by inducing apoptotic depletion of activated pathogenic lymphocytes. J Immunol 2003;170: 2985–2992.
46. Li H, Llera A, Malchiodi EL, Mariuzza RA. The structural basis of T cell activation by superantigens. Annu Rev Immunol 1999;17: 435–466.
47. Andersen PS, Geisler C, Buus S, Mariuzza RA, Karjalainen K. Role of the T cell receptor ligand affinity in T cell activation by bacterial superantigens. J Biol Chem 2001;276:33452–33457.
48. Omoe K, Hu DL, Takahashi-Omoe H, Nakane A, Shinagawa K. Identification and characterization of a new staphylococcal enterotoxin-related putative toxin encoded by two kinds of plasmids. Infect Immun 2003;71:6088–6094.
49. Kravitz GR, Dries DJ, Peterson ML, Schlievert PM. Purpura fulminans due to *Staphylococcus aureus* Clin Infect Dis 2005;40: 941–947.